Gallium Phosphide IMPATT Sources for Millimeter-Wave Applications

A. Acharyya*(C.A.)

Abstract: The potentiality of millimter-wave (mm-wave) double-drift region (DDR) impact avalanche transit time (IMPATT) diodes based on a wide bandgap (WBG) semiconductor material, Gallium Phosphide (GaP) has been explored in this paper. A non-sinusoidal voltage excited (NSVE) large-signal simulation method has been used to study the DC and high frequency characteristics of DDR GaP IMPATTs dsigned to operate at mm-wave atmospheric window frequencies such as 94, 140 and 220 GHz. Results show that the DDR GaP IMPATTs are capable of delivering significantly higher RF power at the above mentioned window frequencies as compared to the DDR IMPATTs based on the conventional narrow bandgap (NBG) base materials such as Si, GaAs and InP.

1 Introduction

IMPACT avalanche transit time (IMPATT) diodes have emerged as the most efficient and convenient two terminal solid-state source for the generation of high RF power with DC to RF conversion efficiency at microwave (3 – 30 GHz) and mm-wave (30 – 300 GHz) frequencies [1-3]. Silicon (having bandgap of $E_g = 1.12$ eV at 300 K) is the most widely used semiconductor base material for the fabrication of IMPATT diodes due to its matured process technology [4-6]. However, some narrow bandgap (NBG) group III-V semiconductors such as GaAs ($E_g = 1.43$ eV at 300 K) and InP ($E_g = 1.35$ eV at 300 K) have also established themselves as powerful and efficient base materials of IMPATT diodes operating at different mm wave atmospheric window frequencies [7-11]. Recently, some researchers have explored the potentiality of a number of wide bandgap (WBG) semiconductors such as 4H-SiC ($E_g = 3.23$ eV at 300 K), 6H-SiC ($E_g = 2.86$ eV at 300 K), 3H-SiC ($E_g = 2.36$eV at 300 K), Wz-GaN ($E_g = 3.40$ eV at

300 K) etc. as the base material of IMPATT diodes capable of delivering high RF power with significantly high DC to RF conversion efficiency at microwave, mm-wave and Terahertz (> 300 GHz) frequency regime [12-16].

In this paper, the authors have explored the potentiality of another WBG semiconductor, i.e. GaP ($E_g = 2.26$ eV at 300 K) as the base material of DDR IMPATT diodes operating and mm-wave window frequencies such as 94, 140 and 220 GHz. A well established non-sinusoidal voltage excitation (NSVE) model based large-signal simulation tool developed by the authors [17-21] has been used to carry out the DC and high frequency simulation of DDR GaP IMPATT diodes designed to operate at abovementioned frequencies. Finally, the large-signal performance of DDR GaP IMPATTs has been compared with that of DDR IMPATTs based on Si, GaAs and InP, in order to verify the superiority of GaP over those conventional base materials.

2 Design and Material Parameters

One-dimensional (1-D) model of the n^+-n-p-p^+ structued DDR IMPATT diode shown in Fig. 1 is taken into account in the present simulation. It may be assumed without any loss of generality or accuracy that the physical phenomena take place in the semiconductor bulk along the symmetry axis (i.e. x-axis) of the device duing IMPATT operation under reverse bias. No
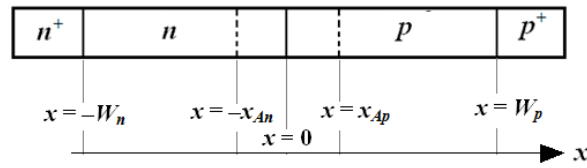
Fig. 1 One-dimensional (1-D) model of the n^+-n-p-p^+ structued DDR IMPATT diode.

Table 1 Design parameters.

Design frequency, f_d	94.00 GHz	140.00 GHz	220.00 GHz
Thickness of the n-epitaxial layer, W_n	1.125 μm	0.800 μm	0.510 μm
Thickness of the p-epitaxial layer, W_p	1.125 μm	0.800 μm	0.510 μm
Donor concentration of the n-epitaxial layer, N_D	0.300×10^{23} m^{-3}	0.480×10^{23} m^{-3}	0.800×10^{23} m^{-3}
Acceptor concentration of the p-epitaxial layer, N_A	0.400×10^{23} m^{-3}	0.680×10^{23} m^{-3}	1.150×10^{23} m^{-3}
Donor concentration of the n^+-contact layer, N_{n+}	5.000×10^{25} m^{-3}	5.000×10^{25} m^{-3}	5.000×10^{25} m^{-3}
Acceptor concentration of the p^+-contact layer, N_{p+}	2.700×10^{25} m^{-3}	2.700×10^{25} m^{-3}	2.700×10^{25} m^{-3}
Junction diameter, D_j	35.00 μm	25.00 μm	20.00 μm
Bias current density, J_0	2.50×10^8 A m^{-2}	5.10×10^8 A m^{-2}	9.40×10^8 A m^{-2}

potential and density gradients are present along other two directions (i.e. along *y*- and *z*-axes) and therefore, carrier transport only takes place along x-axis. Thus the consideration of 1-D model is absolutely justified [22,23]. The realistic doping profile of the device is taken into account by incorporating appropriate exponential function near *n-p* metallurgical junction and appropriate error functions near n^+-*n* and p^+-*p* interfacs [24]. The design parameters such as widths of *n*- and *p*-epitaxial layers (i.e. W_n and W_p), corresponding doping concentrations (i.e. N_D and N_A) and optimum bias current density (J_0) for IMPATT operation at a particular design frequency (f_d) are chosen by using a organized trial and error method reported earlier by the authors [17]. The design parameters of 94, 140 and 220 GHz DDR GaP IMPATTs are given in Table 1.

The realistic field dependent ionization rates ($α_n$, $α_p$), the field dependent drift velocities (v_n, v_p), field dependent mobilities ($μ_n$, $μ_p$) and other material parameters such as bandgap (E_g), intrinsic carrier concentration (n_i), effective density of states of conduction and valance bands (N_c, N_v), effective masses (m_n^*, m_p^*), diffusion coefficients (D_n, D_p) and diffusion lengths (L_n, L_p) of charge carriers in GaP at 300 K are incorporated in the simulation program from recently published reports [25-30].

3 Simulation Technique

The complete RF performance of DDR IMPATT diode can be studied by carrying out DC simulation followed by large-signal simulation. The design frequency, structural and doping parameters, bias current density and all material parameters are entered as the input of the simulation program. At first, the DC simulation is carried out by solving the fundamental space dependent device equations such as Poisson's equation, carrier continuity equations and current density equations simultaneously subject to appropriate

field and current boundary conditions at depletion layer edges by using finite difference method (FDM) [17-21]. The simultaneous numerical solution of the abovementioned equations provides DC outcomes such as spatial variations of electric field, electric potential, electron and hole components of the current density, electron and hole concentrations, etc. within the depletion layer as well as breakdown voltage (V_B), avalanche voltage drop (V_A), avalanche region width (x_A), etc. as functions of bias current density.

In the next step, the time variation in the terminal voltage across the reverse biased diode is introduced by a non-sinusoidal RF waveform having form $v_{rf}(t) = V_B(m_x \sin(2\pi f_d t) + m_x^2 \sin(4\pi f_d t) + m_x^3 \sin(6\pi f_d t) + … + m_x^z \sin(2z\pi f_d t))$ with a fundamental frequency (f_d) term along with ($z - 1$) number of harmonics; where mx is the percentage of modulation of the RF waveform over V_B. The time variation $v_{rf}(t)$ introduces time variations in the aforementioned device equations. Therefore, by solving those time and space dependent device equations subject to appropriate time dependent field and current boundary conditions at depletion layer edges for different values of m_x ranging from 0 – 70%, the corresponding terminal current ($i_T(t)$) waveforms are obtained. The value $m_x = 0\%$ is corresponding to no time variation, i.e. DC simulation; whereas $m_x > 0\%$ values provide time varying solutions of $i_T(t)$. On the other hand, time varying terminal voltage ($v_T(t)$) for each mx values are obtained by integrating corresponding time and space dependent electric field ($ξ(x,t)$) with respect to *x* within the depletion layer (i.e. from $x = -W_n$ to $x = W_p$). The value of m_x should not be increased beyond 70%, because over-modulation causes significant decrease in electric field during negative half cycles of the oscillation, which, in turn, degrades the field dependent material parameters in large extent and consequently causes deterioration in large-signal performance of the device. The device system is made time dependent by introducing non-sinusoidal

waveform $v_{rf}(t)$ at the starting point, that is why this method is called non-sinusoidal voltage excitation (NSVE) model for large-signal simulation.

Now the time domain $v_T(t)$ and $i_T(t)$ are Fourier transformed in order to obtain the frequency domain $v_T(f)$ and $i_T(f)$. After that the diode admittance as function of frequency is obtained as $Y_d(f) = I_T(f)/V_T(f)$. Decomposing the real and imaginary parts of $Y_d(f) = G(f) + j\,B(f)$, provides the knowledge of conductance ($G(f)$) and susceptance ($B(f)$) as functions of frequency. The frequency at which $G(f)$ changes sign from positive to negative, is called avalanche resonance frequency (f_a). IMPATT operation starts when the frequency is increased above fa and the device becomes capable of

delivering RF power to the load. Ultimately, the RF power output ($P_{RF} = (1/2)(m_x V_B)^2|G_p|A_j$) and DC to RF conversion efficiency ($\eta_L = P_{RF}/P_{DC}$; where $P_{DC} = J_0 V_B A_j$) are obtained as the outcome of the large-signal program as functions of mx; where $|G_p|$ is the peak magnitude of the negative conductance corresponding to the optimum frequency (f_p) of operation, $A_j = \pi(D_j/2)^2$ is the junction area (D_j is the diameter of the junction having circular cross-section) [17-21]. The value of m_x is kept 5% during the first run of the large-signal program and it is increased by a step $\Delta m_x = 5\%$ after each run of it. Finally the large-signal program is terminated when mx reaches 70%. The complete flowchart of the simulation program is shown in Fig. 2.
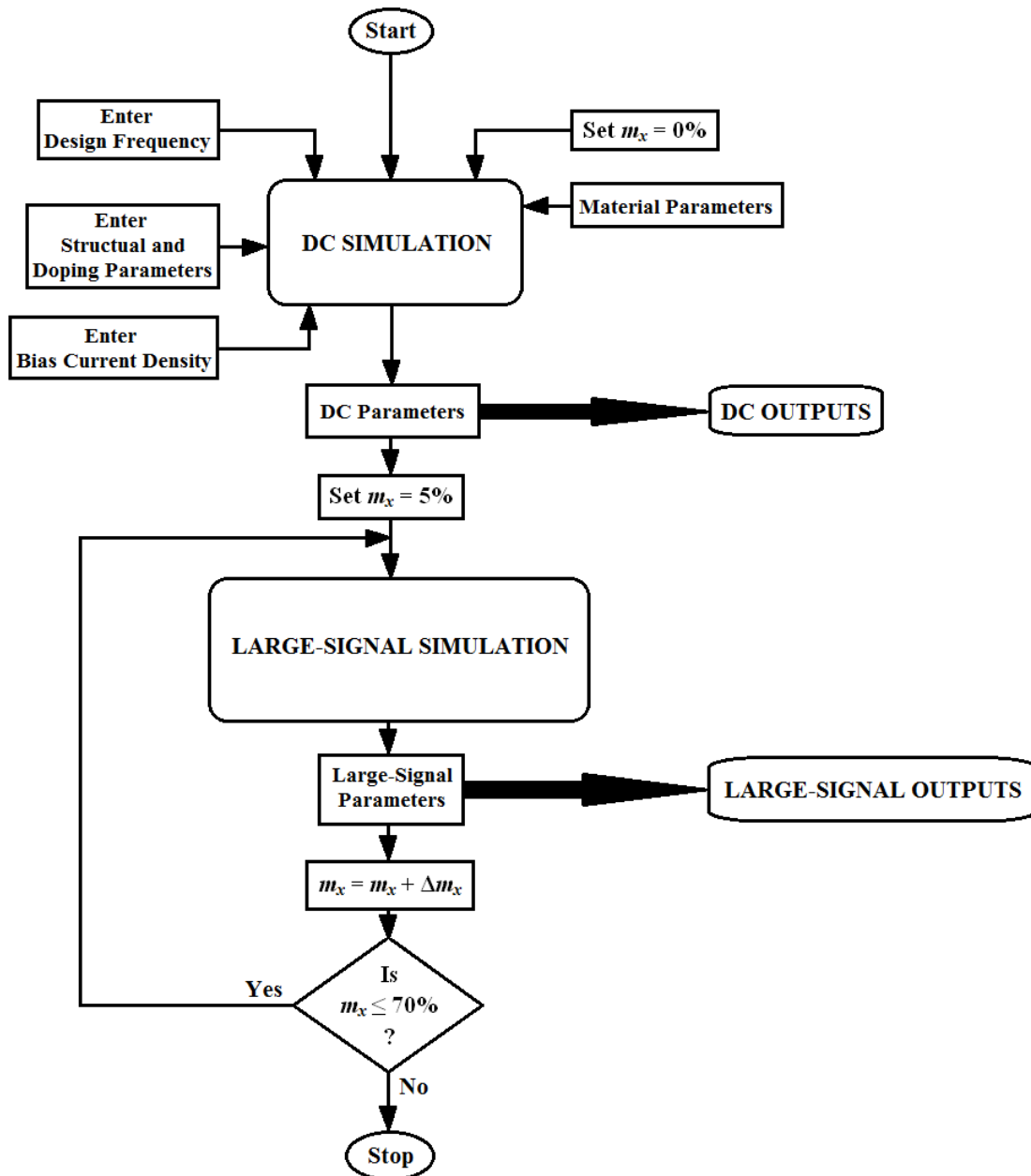

Fig. 2 Flowchart of the simulation program.

4 Results and Discussion

The simulation method described above has been used to study the DC and large-signal properties of DDR GaP IMPATT diodes designed to operate at 94, 140 and 220 GHz frequencies. The simulations have been carried out for the bias current densities ranging from $2.0 \times 10^8 - 3.0 \times 10^8$, $4.5 \times 10^8 - 5.5 \times 10^8$ and $9.0 \times 10^8 - 10.0 \times 10^8$ A m^{-2} corresponding to 94, 140 and 220 GHz diodes. The range of the bias current density for a diode has been chosen for which the diode possesses negative conductance (i.e. the real part of the diode admittance $G(f)$ is negative); that means for any value of bias current density smaller or larger than the range provided here, the respective diode possesses positive conductance (i.e. real part of the diode impedance $G(f)$ is positive) which is corresponding to non-oscillating condition and it will not able to deliver RF power to the load.

4.1 DC Characteristics

The electric field profiles of the diodes operating at 94, 140 and 220 GHz frequencies corresponding to the optimum bias current densities of 2.5×10^8, 5.1×10^8 and 9.4×10^8 A m^{-2} obtained from the DC simulation are shown in Fig. 3. It is observed that peak electric field increases significantly with the increase of operating frequency. It is obvious, since the thickness of the active region of IMPATT diode (i.e. $W = W_n + W_p$) decreases (see Table 1) in order to support higher frequency of operation; which leads to narrower depletion region width and larger peak electric field at the metallurgical junction in higher frequency diodes.

Variations of important DC parameters such as peak electric field (ξ_p), breakdown voltage (V_B), avalanche zone voltage drop (V_A), ratio of drift zone voltage drop ($V_D = V_B - V_A$) to breakdown voltage (V_D/V_B), avalanche region width (x_A) and ratio of avalanche zone width to total depletion region width (x_A/W), etc. of the diodes with bias current density (J_0) have been shown in Figs. 4 (a) – (i). It is observed from Figs. 4 (a) – (c) that ξ_p decreases slightly from $7.1979 \times 10^7 - 7.1493 \times 10^7$, $7.6532 \times 10^7 - 7.6143 \times 10^7$ and $8.2306 \times 10^7 - 8.1932 \times 10^7$ V m^{-1} in 94, 140 and 220 GHz DDRs for increment of the J_0 from $2.0 \times 10^8 - 3.0 \times 10^8$, $4.5 \times 10^8 - 5.5 \times 10^8$ and $9.0 \times 10^8 - 10.0 \times 10^8$ A m^{-2} respectively. Due to the presence of higher amount of space charges in the depletion region of a reverse biased IMPATT diode at higher current densities, peak electric field at the *p-n* junction decreases, however electric field at each space point within the depletion layer away from the junction slightly increases [31, 32]; even the diode may become highly punch through at higher bias current densities. Figures 4 (d) – (f) show the variations of V_B, V_A and V_D/V_B of the diodes with J_0. Higher current through the device causes larger voltage drop across the depletion layer, which, in turn, increases the break down voltage (V_B). The value of V_B increases from 85.90 – 90.68,

62.63 – 65.11 and 44.65 – 44.99 V in 94, 140 and 220 GHz diodes respectively for the increment of abovementioned ranges of J_0. The changes of V_A and V_D/V_B are observed to be 40.01 – 43.92, 30.88 – 32.35 23.10 – 24.36 V and 53.42 – 51.57, 50.69 – 51.31, 48.26 – 45.85% respectively. The avalanche region or multiplication region of the device has to be expanded in order to accommodate increased amount of carrier multiplications due to increased bias current density. Therefore, the avalanche region width (x_A) has to be greater for greater bias current density. Variations of x_A ($x_A = |x_{An}| + x_{Ap}$; see Fig. 1) and x_A/W of the diodes with bias current density are shown in Figs. 4 (g) – (i) which are clearly depicting the broadening of avalanche region with the increase of bias current density. Obviously, greater voltage drop occurs across the wider avalanche regions at higher bias current densities; as a result V_A increases with the increase of J_0 as depicted earlier. The drift region width $V_D = V_B - V_A$ decreases with the increase of J_0 since the rate of increase of V_A with respect to J_0 is found to be slightly higher as compared to that of V_B; thus the ratio V_D/V_B decreases with the increase of J_0. The ratio V_D/V_B determines the DC to RF conversion efficiency of the diode as per the semi-quantitative formula reported earlier [33].

4.2 Large-Signal Characteristics

Variations of important large-signal parameters such as avalanche resonance frequency (f_a), optimum frequency (f_p), magnitude of the peak negative conductance ($|G_p|$), corresponding susceptance (B_p), quality factor or Q-factor ($Q_p = -B_p/G_p$) and peak magnitude of the negative resistance ($|Z_R| = |G_p/(G_p^2 + B_p^2)|$) of the diodes for $m_x = 50\%$ with bias current
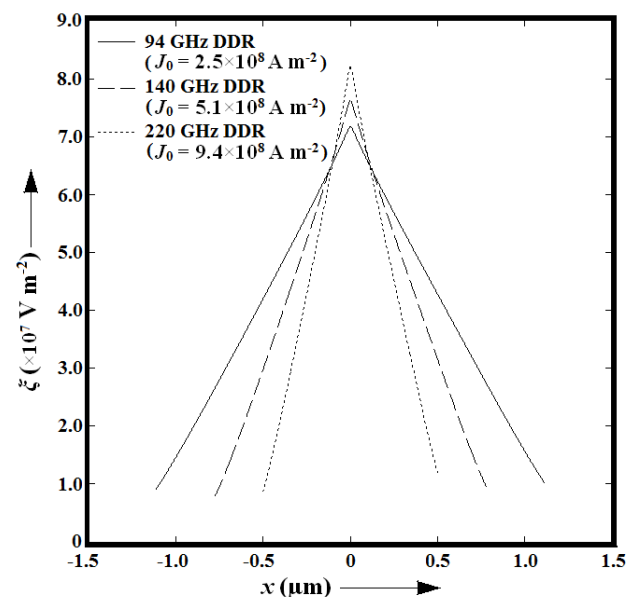

Fig. 3 Electric field profiles of the DDR GaP IMPATT diodes designed to operate at 94, 140 and 220 GHz for the bias current densities of 2.5×10^8, 5.1×10^8 and 9.4×10^8 A m^{-2} respectively.
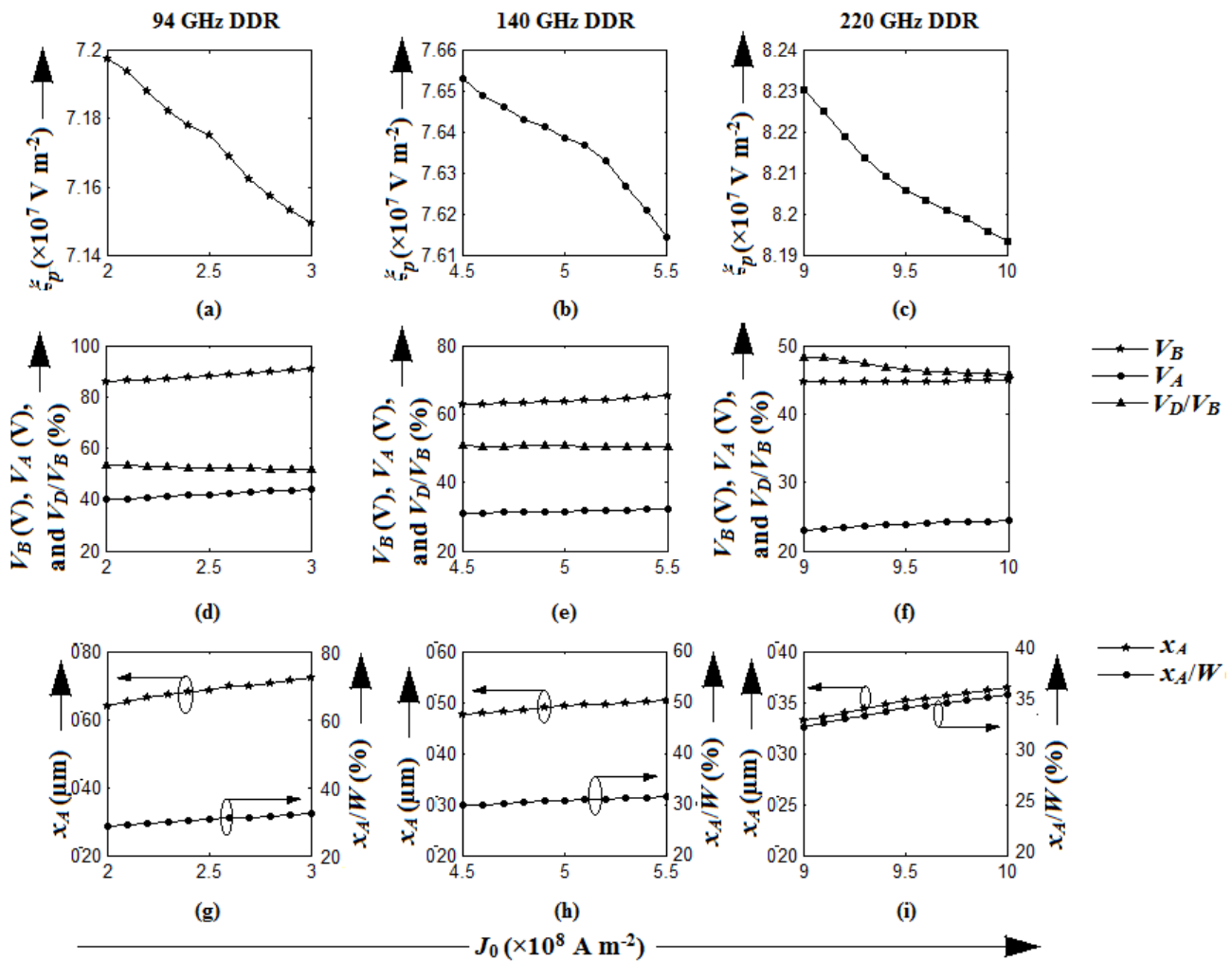
Fig. 4 Variations of static parameters of 94, 140 and 220 GHz DDR GaP IMPATT diodes with bias current density.

density have been shown in Figs. 5 (a) – (i). Sharp increase of f_p is observed from 87.50 – 97.90, 135.20 – 142.10 and 214.70 – 225.70 GHz in 94, 140 and 220 GHz diodes for the increase of bias current density of $2.0 \times 10^8 – 3.0 \times 10^8$, $4.5 \times 10^8 – 5.5 \times 10^8$ and $9.0 \times 10^8 – 10.0 \times 10^8$ A m^{-2} respectively. However, the increase of f_a is found to be 47.60 – 54.20, 77.10 – 83.40 and 113.70 – 123.00 GHz in those diodes with the same increase of J_0, which are less sharp as compared to f_p versus J_0. Greater bias current causes greater amount of space charge effect [31, 32] and as a result the electric field at each space point away from the junction increases as mentioned earlier. Greater electric field at the majority portion of the depletion layer especially near the depletion layer edges increases carrier drift velocity (since near the depletion layer edges field value are not so high that the carrier drift velocity reaches its saturation value (see Fig. 3)), since unsaturated carrier drift velocities are monotonically increasing functions of electric field [28]; consequently, the carriers need less transit time to travel from one to another electrode, which leads to increase in both f_p and f_a. Increment in

bias current density causes increment in the admittance of the device; thus both the magnitudes of the negative conductance and susceptance must increase with the increase of bias current density. Figures 5 (d) – (f) show that both $|G_p|$ and B_p increase with the increase of J_0.

Admittance characteristics of 94, 140 and 220 GHz diodes for the optimum bias current densities of 2.5×10^8, 5.1×10^8 and 9.4×10^8 A m^{-2} have been shown in Fig. 6. Optimum values of G_p and B_p are found to be – 0.1315×10^7, $–0.3019 \times 10^7$, $–0.6439 \times 10^7$ S m^{-2} and 0.5573×10^7, 1.1504×10^7, 2.8326×10^7 S m^{-2} respectively corresponding to the abovementioned optimum bias current densities. Moreover, the optimum values of f_a and f_p are found to be 51.90, 82.10, 119.60 GHz and 93.60, 140.10, 220.40 GHz respectively. The Q-factor of the diodes remains around 4.0 for all bias current densities under consideration. On the other hand, it is noteworthy from Figs. 5 (g) – (i) that $|Z_R|$ increases with the increase of bias current density which indicates the increase of RF power output with the increment of J_0. However, $|Z_R|$ decreases sharply with the increase of operating frequency of the device; this fact is the cause
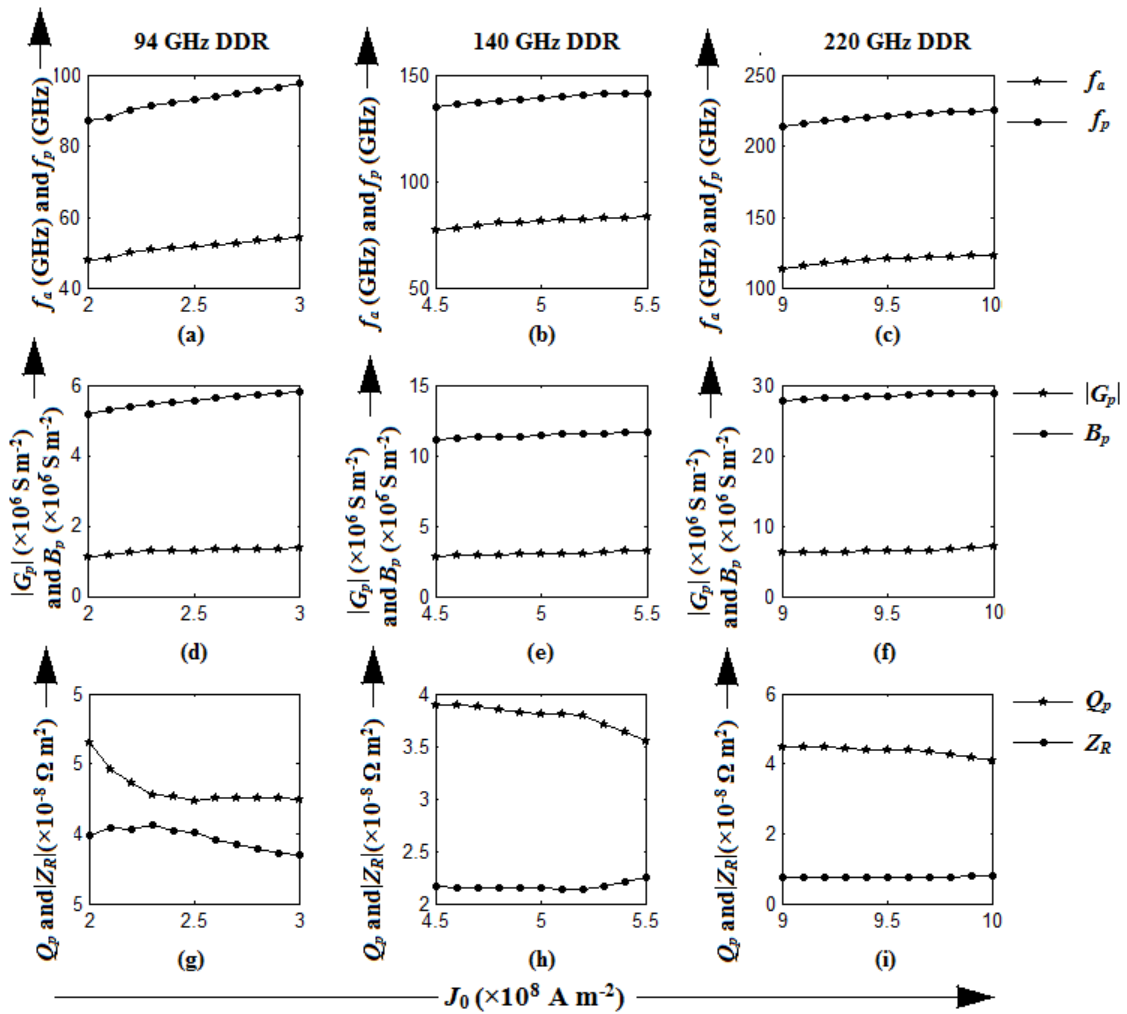
Fig. 5 Variations of large-signal parameters of 94, 140 and 220 GHz DDR GaP IMPATT diodes with bias current density.
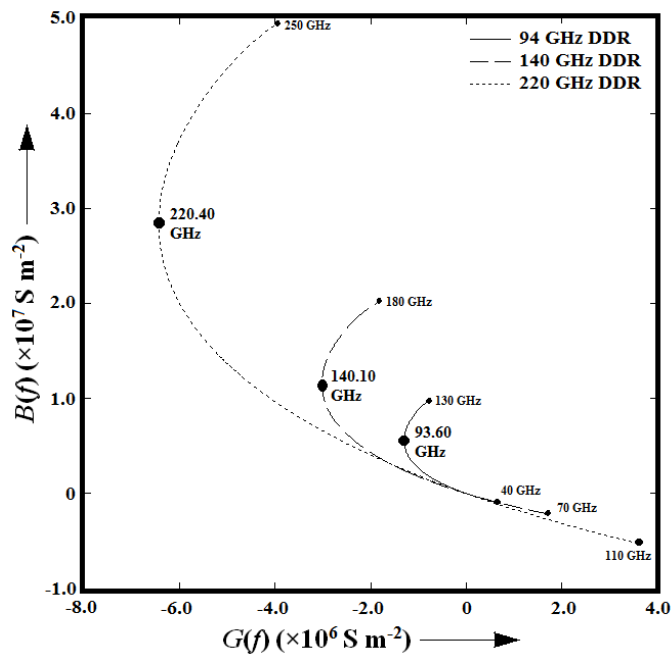

Fig. 6 Admittance characteristics of 94, 140 and 220 GHz DDR GaP IMPATT diodes for the bias current densities of 2.5×10^8, 5.1×10^8 and 9.4×10^8 A m^{-2} respectively.

of sharp decay of RF power output at higher mm-wave frequencies.

The variations of P_{RF} and η_L of 94, 140 and 220 GHz diodes with bias current density are shown in Figs. 7 (a) and (b) respectively. Monotonically increasing P_{RF} with J_0 is observed for all the diodes under consideration; it is obvious, since both V_B and $|G_p|$ are monotonically increasing functions of J_0 which have been already illustrated in Figs. 4 (d) – (f) and 5 (d) – (f). However, variations of η_L with J_0 are found to be (a) initially increasing up to 6.09% for $2.20{\times}10^8$ A m^{-2}, after which monotonically decreasing till $3.00{\times}10^8$ A m^{-2} in 94 GHz diode, (b) initially decreasing up to 4.69% for $5.20{\times}10^8$ A m^{-2}, after which monotonically increasing till $5.50{\times}10^8$ A m^{-2} in 140 GHz diode and (c) initially decreasing up to 3.80% for $9.70{\times}10^8$ A m^{-2}, after which monotonically increasing till $10.00{\times}10^8$ A m^{-2} in 220 GHz diode.

Since now, all the large-signal parameters presented in this paper are for $m_x = 50\%$. Simulations have also been carried out by varying the m_x from 5.0 – 70.0% in order to study the variations of large-signal parameters with RF voltage ($V_{RF} = m_x V_B$). Variations of P_{RF} and η_L of the DDR GaP IMPATTs with V_{RF} for the corresponding optimum bias current densities have been shown in Figs. 7 (c) and (d). It is interesting to observe from Fig. 7 (c) that P_{RF} initially increases with the increase of V_{RF} and attains its peak when m_x reaches 60%. Then P_{RF} decreases sharply with further increase of m_x beyond 60%. The nature of η_L vs. V_{RF} also shows the same nature. The degradation of P_{RF} and η_L at voltage

modulation factors larger than 60% occurs due to the deterioration of field dependent material parameters at very low electric fields during negative half cycles of the RF voltage swing. Therefore, the value of the voltage modulation factor must be within 50 – 60% in order to obtain highest RF power output from the device with maximum DC to RF conversion efficiency.

4.3 Comparison with IMPATT Sources Based on Si, GaAs and InP

Variations of RF power output of IMPATT sources based on GaP as well as some conventional base materials such as Si, GaAs and InP with operating frequency have been shown in Fig. 8. It is interesting to observe from Fig. 8 that DDR GaP IMPATT diodes are capable of delivering much higher RF power (1.23 W, 757.34 mW and 505.43 mW) as compared to their Si (653.35, 378.89 and 297.50 mW) [19] and GaAs (781.37, 227.02 and 177.77 mW) [34] counterparts at 94, 140 and 220 GHz window frequencies respectively. DDR InP IMPATT diode delivers slightly higher RF power (1.33 W) at 94 GHz as compared to DDR GaP IMPATT operating at that frequency [34]. However, DDR GaP IMPATTs excel its InP counterparts (719.97 and 440.93 mW) at higher mm-wave frequencies, i.e. at 140 and 220 GHz respectively [34]. Therefore, GaP is the more preferable material over conventional base materials such as Si, GaAs and InP for fabricating DDR IMPATTs, especially at higher mm-wave frequencies (>100 GHz).
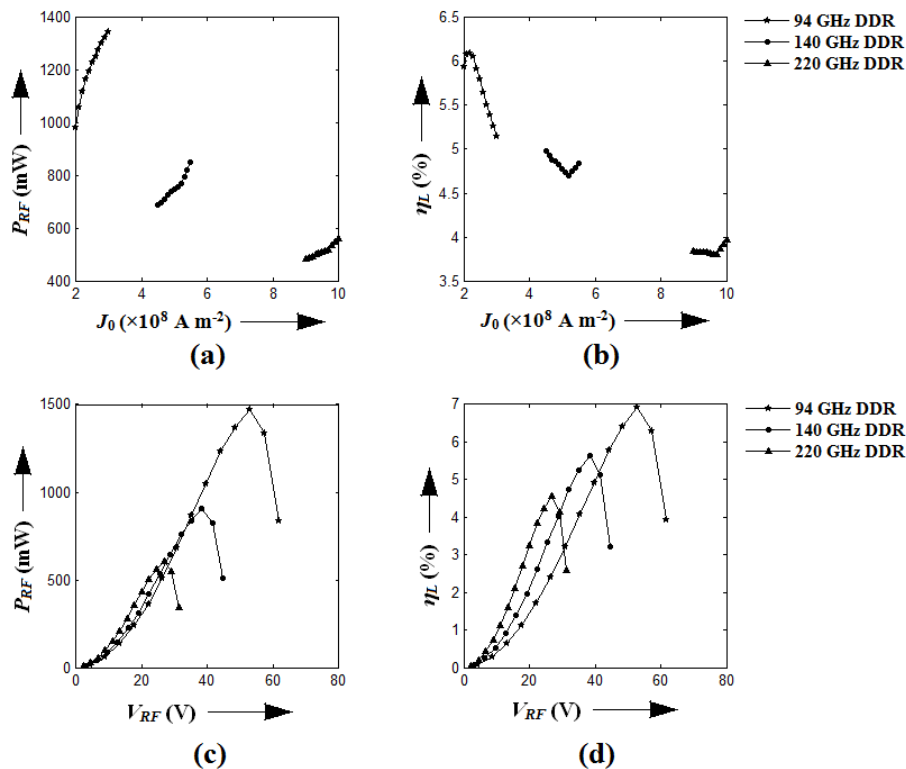
Fig. 7 Variations of RF power output and DC to RF conversion efficiency of 94, 140 and 220 GHz DDR GaP IMPATT diodes with (a), (b) bias current density and (c), (d) RF voltage respectively.
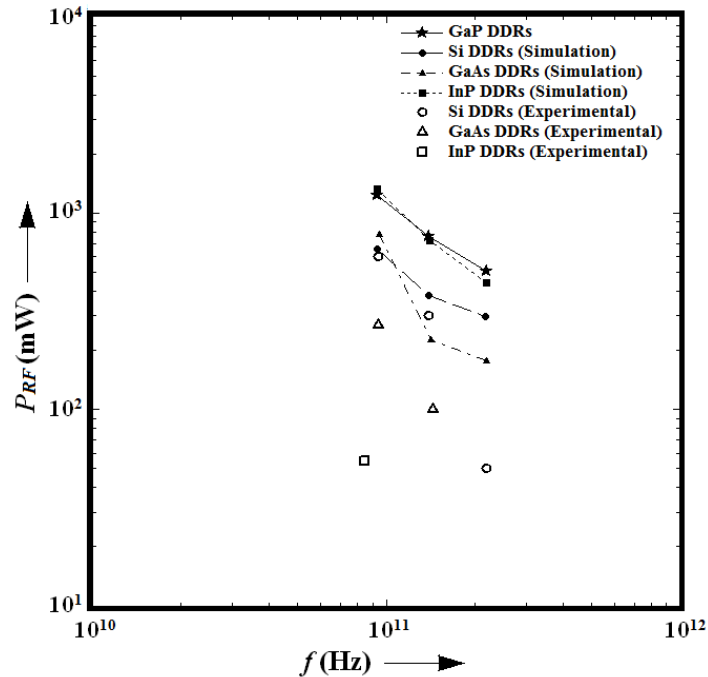
Fig. 8 Variations of RF power output of DDR IMPATT diodes based on GaP, Si, GaAs and InP with operating frequency obtained from both NSVE large-signal simulation [19,34] and experiments [1,4,6,7,10,11].

4.4 Validation of the Simulation Results

Experimentally obtained RF power outputs from DDR IMPATTs sources based on Si, GaAs and InP have been shown in Fig. 8. Experimental RF power outputs from DDR Si IMPATT oscillators are 600, 300 and 50 mW at 94, 140 and 220 mW respectively [1,4,6]. Experimental RF power output from DDR GaAs IMPATTs are 270 and 100 mW at 95 and 144 GHz respectively [7,10] and same from DDR InP IMPATT source is 55 mW at 84.8 GHz [11]. It is noteworthy from Fig. 8 that the NSVE large-signal simulation results are in close agreement with experimental results in most of the cases. Discrepancy observed in between simulation experimental results in case of 220 GHz Si DDR and DDRs based on GaAs and InP are due to lack of matured process technology and un-optimized design parameters used for fabrication of those diode for those experiments [1,4,6,7,10,11]. So far as authors' knowledge is concerned, no experimental report on the RF performance of DDR GaP IMPATTs is available in published literature and so the comparison with simulation results cannot be made.

5 Conclusion

The potentiality of mm-wave DDR IMPATTs based on GaP have been explored in this paper. Comprehensive DC and large-signal simulations have been carried out on DDR GaP IMPATT diodes design to operate at 94, 140 and 220 GHz mm-wave window frequncies for this purpose and results have presented in the forms of necessay graphs or plots. Results show that the DDR GaP IMPATTs are capable of deliveing

considerably higher RF power at mm-wave atmospheric window frequencies as compared to their conventional counterparts such as DDR IMPATTs based on Si, GaAs and InP. Optimum design parameters and simulation results presented in this paper will be useful for fabricating mm-wave DDR GaP IMPATT diodes by using either molecular beam epitaxy (MBE) or metalorganic chemical vapour deposition (MOCVD) technique.

Acknowledgement

References

[1] T. A. Midford and R. L. Bernick, "Millimeter wave CW IMPATT diodes and oscillators," *IEEE Transactions on Microwave Theory Technology*, Vol. 27, No. 5, pp. 483-492, 1979.

[2] W. W. Gray, L. Kikushima, N. P. Morentc and R. J. Wagner, "Applying IMPATT power sources to modern microwave systems," *IEEE Journal of Solid-State Circuits*, Vol. 4, No. 6, pp. 409-413, 1969.

[3] Y. Chang, J. M. Hellum, J. A. Paul and K. P. Weller, "Millimeter-wave IMPATT sources for communication applications," *IEEE MTT-S International Microwave Symposium Digest*, pp. 216-219, 1977.

[4] J. F. Luy, A. Casel, W. Behr and E. Kasper, "A 90-GHz double-drift IMPATT diode made with Si MBE," *IEEE Transactions on Electron Devices*, Vol. 34, No.5, pp. 1084-1089, 1987.

[5] C. Dalle, P. Rolland and G. Lieti, "Flat doping profile double-drift silicon IMPATT for reliable CW high power high-efficiency generation in the 94-GHz window," *IEEE Transactions on Electron Devices*, Vol. 37, No. 1, pp. 227-236, 1990.

[6] M. Wollitzer, J. Buchler, F. Schafflr and J. F. Luy, "D-band Si-IMPATT diodes with 300 mW CW output power at 140 GHz," *Electronics Letters*, Vol. 32, No. 2, pp. 122-123, 1996.

[7] H. Eisele, "Selective etching technology for 94 GHz, GaAs IMPATT diodes on diamond heat sinks," *Solid State Electronics*, Vol. 32, No. 3, pp.253-257, 1989.

[8] H. Eisele, "GaAs W-band IMPATT diode for very low noise oscillations," *Electronics Letters*, Vol.26, No. 2, pp. 109-110, 1990.

[9] H. Eisele and G. I. Hadded, "GaAs single-drift flat profile IMPATT diodes for CW operation at D band," *Electronics Letters*, Vol. 28, No. 23, pp. 2176-2177, 1992.

[10] M. Tschernitz and J. Freyer, "140 GHz GaAs double-Read IMPATT diodes," *Electronics Letters*, Vol. 31, No. 7, pp. 582-583, 1995.

[11] H. Eisele, C. C. Chen, G. O. Munns and G. I. Haddad, "The potential of InP IMPATT diodes as high-power millimetre-wave sources: first experimental results," *IEEE MTT-S International Microwave Symp. Digest*, Vol. 2, pp 529-532, 1996.

[12] A. Acharyya and J. P. Banerjee, "Prospects of IMPATT devices based on wide bandgap semiconductors as potential terahertz sources," *Applied Nanoscience*, Vol. 4, No. 1, pp. 1-14, 2014.

[13] A. Acharyya and J. P. Banerjee, "Potentiality of IMPATT devices as terahertz source: An avalanche response time based approach to determine the upper cut-off frequency limits," *IETE Journal of Research*, Vol. 59, No. 2, pp. 118-127, 2013.

[14] L. Yuan, A. James, J. A. Cooper, M. R. Melloch and K. J. Webb, "Experimental demonstration of a silicon carbide IMPATT oscillator," *IEEE Electron Device Letter*, Vol. 22, No. 6, pp. 266-268, 2001

[15] K. V. Vassilevski, A. V. Zorenko, K. Zekentes, K. Tsagaraki, E. Bano, C. Banc and A. Lebedev, "4H-SiC IMPATT diode fabrication and testing," *Technical Digest of International Conference on SiC and Related Materials, Tsukuba, Japan*, pp. 713-714, 2001.

[16] R. J. Trew, J. B. Yan and P. M. Mock, "The potentiality of diamond and SiC electronic devices for microwave and millimeter-wave power applications," *Proc. of IEEE*, Vol. 79, No. 5, pp. 598-620, 1991.

[17] A. Acharyya, S. Banerjee and J. P. Banerjee, "Effect of junction temperature on the large-signal properties of a 94 GHz silicon based double-drift region impact avalanche transit time device," *Journal of Semiconductors*, Vol. 34, No. 2, pp. 024001-12, 2013.

[18] A. Acharyya, S. Banerjee and J. P. Banerjee, "A proposed simulation technique to study the series resistance and related millimeter-wave properties of Ka-band Si IMPATTs from the electric field snap-shots," *International Journal of Microwave and Wireless Technologies*, Vol. 5, No. 1, pp. 91-100, 2013.

[19] A. Acharyya, J. Chakraborty, K. Das, S. Datta, P. De, S. Banerjee and J. P. Banerjee, "Large-signal characterization of DDR silicon IMPATTs operating up to 0.5 THz," *International Journal of Microwave and Wireless Technologies*, Vol. 5, No. 5, pp. 567-578, 2013.

[20] A. Acharyya, S. Banerjee and J. P. Banerjee, "Influence of skin effect on the series resistance of millimeter-wave of IMPATT devices," *Journal Computational Electronics*, Vol. 12, No. 3, pp. 511-525, 2013.

[21] P. K. Bandyopadhyay, S. Chakraborty, A. Biswas, A. Acharyya and A. K. Bhattacharjee, "Large-signal characterization of millimeter-wave IMPATTs: effect of reduced impact ionization rate of charge carriers due to carrier-carrier interactions," *Journal of Computational Electronics*, Vol. 15, No. 2, pp. 646-656, 2016.

[22] M. S. Sorokin and A.V. Arkhipov, "Analysis of the thermal conditions of pulse impact avalanche transit-time diodes," *J. Nano-Electron. Physics*, Vol. 1, No. 4, pp. 76-80, 2009.

[23] J. L. Blue, "Approximate large-signal analysis of IMPATT oscillators," *Bell system technical journal*, Vol. 48, No. 2, pp. 383-396, 1969.

[24] Aritra Acharyya, "RF performance of IMPATT sources and their optical control," *Lambert Academic Publishing, Germany*, 2015.

[25] A. S. Kyuregyan and S. N. Yurkov, "Room-temperature avalanche breakdown voltages of p-n junctions made of Si, Ge, SiC, GaAs, GaP, and InP," *Sov. Physics Semiconductors*, Vol. 23, No. 10, pp. 1126, 1989.

[26] M. L. Young and D. R. Wight, "Concentration dependence of the minority carrier diffusion length and lifetime in GaP," *Journal of Physics D*, Vol. 7, No. 13, pp. 1824, 1974.

[27] V. K. Arora, D. S. L. Mui and H. Morkoc, "High-field electron-drift velocity and temperature in gallium phosphide," *Journal of applied physics*, Vol. 61, No. 9, pp. 4703-4704, 1987.

[28] R. H. Johnson and O. Eknoyan, "High-field electron drift velocity measurements in gallium phosphide," *Journal of applied physics*, Vol. 58, No.3, pp. 1402-1403, 1985.

[29] Y. O. Kao and O. Eknoyan, "Electron and hole carrier mobilities for liquid phase epitaxially grown GaP in the temperature range 200-550 K," *Journal of applied physics*, Vol. 54, No. 5, pp. 2468-2471, 1983.

[30] "Electronic archive: new semiconductor materials, characteristics and properties", http://www.ioffe.ru/SVA/NSM/Semicond/index.html.

[31] M. Sridharan and S. K. Roy, "Computer studies on the widening of the avalanche zone and decrease on efficiency in silicon X-band symmetrical DDR," *Electronics Letters*, Vol. 14, No. 19, pp. 635-637, 1978.

[32] M. Sridharan and S. K. Roy, "Effect of mobile space charge on the small signal admittance of silicon DDR," *Solid State Electronics*, Vol. 23, No. 9, pp. 1001-1003, 1980.

[33] D. L. Scharfetter and H. K. Gummel, "Large-signal analysis of a silicon read diode oscillator," *IEEE Transactions on Electron Devices*, Vol. 6, No. 1, pp. 64-77, 1969.

[34] A. Acharyya, A. Mallik, D. Banerjee, S. Ganguli, A. Das, S. Dasgupta and J. P. Banerjee, "IMPATT devices based on group III-V compound semiconductors: prospects as potential terahertz radiators," *HKIE Transactions*, Vol. 21, No. 3, pp. 135-147, 2014.

A. Acharyya was born in 1986. He received Ph.D. and M.Tech. degrees from the Institute of Radio Physics and Electronics, University of Calcutta, Kolkata, India, in the years of 2016 and 2010 respectively. Earlier he received B.E. degree in Electronics and Telecommunication Engineering from Bengal Engineering and Science University, Shibpur, WB, India, in the year of 2007. Currently, he has been working as an Assistant Professor of Electronics and Communication Engineering Department of Cooch Behar Government Engineering College, West Bengal, India. His research interests are semiconductor devices and transport phenomena. He has published more than 120 research papers in peer reviewed journals and conference proceedings.